AGU ADVANCING EARTH AND SPACE SCIENCE

Geophysical Research Letters

COMMENTARY
10.1029/2022GL101408

This article is a commentary on Rheinlænder et al. (2022), https://doi.org/10.1029/2022GL099024.

Key Points:

- Observational data provide context for a 2013 Beaufort Sea (BS) breakout simulated with the neXtSIM model by Rheinlænder et al. (2022, https://doi.org/10.1029/2022GL099024)
- While the 2013 event was exceptional, winter sea ice breakout is common under anticyclonic winds including in years with thicker ice packs
- Wind direction relative to the coast influences the timing and location of lead opening during breakout in the BS

Supporting Information:

Supporting Information may be found in the online version of this article.

Correspondence to:

M. E. Jewell,
jewellm@oregonstate.edu

Citation:

Jewell, M. E., & Hutchings, J. K. (2023). Observational perspectives on Beaufort Sea ice breakouts. *Geophysical Research Letters*, *50*, e2022GL101408. https://doi.org/10.1029/2022GL101408

Received 29 SEP 2022
Accepted 19 DEC 2022

Author Contributions:

Conceptualization: MacKenzie E. Jewell, Jennifer K. Hutchings
Formal analysis: MacKenzie E. Jewell
Funding acquisition: MacKenzie E. Jewell, Jennifer K. Hutchings
Methodology: MacKenzie E. Jewell
Project Administration: Jennifer K. Hutchings
Supervision: Jennifer K. Hutchings
Visualization: MacKenzie E. Jewell
Writing – original draft: MacKenzie E. Jewell

Observational Perspectives on Beaufort Sea Ice Breakouts

MacKenzie E. Jewell[1] and Jennifer K. Hutchings[1]

[1]College of Earth, Ocean, and Atmospheric Sciences, Oregon State University, Corvallis, OR, USA

Abstract In winter 2013, a sea ice breakout in the Beaufort Sea produced extensive fracturing and contributed to record ice export. Rheinlænder et al. (2022, https://doi.org/10.1029/2022GL099024) simulated this event using the neXtSIM sea ice model, reproducing a realistic progression of lead opening and ice drift following the track of an anticyclone. Their simulations indicate strong winds and thin ice are key factors in breakouts. We discuss observational records giving additional insight into the mechanisms controlling breakout events, including the role of wind direction. Breakouts are common and have occurred under weaker winds than in 2013 and in thicker ice of previous decades. During 2013 and other events, patterns of lead opening during breakout followed changes in wind direction relative to the coast with anticyclone position. For skillful predictions of future breakouts, models must reproduce this behavior, and their performance should be assessed across a range of wind and ice conditions.

Plain Language Summary In winter, the Beaufort Sea is covered by a layer of sea ice that is usually frozen against the southern and eastern coastlines that bound the sea. When winds continuously blow from east to west away from these boundaries, the ice cover can tear apart and rapidly drift away from the coasts in what is called a breakout event. The prediction of such dynamic events is important for those who navigate the region. Rheinlænder et al. (2022, https://doi.org/10.1029/2022GL099024) recently used the neXtSIM sea ice model to simulate realistic ice cracking and drift during an exceptionally strong breakout that occurred in 2013. The authors highlighted strong winds and thin sea ice as key factors for breakout. We use observational records to provide additional insight into processes during Beaufort breakouts. Records of many similar events demonstrate that breakouts are common under weather patterns that produce east-to-west winds, even for weaker winds and thicker ice than in 2013. Across observed events, wind direction influences sea ice fracturing patterns and breakout timing. To ensure that model predictions of future sea ice breakouts are accurate, simulations should be compared against observations of multiple recorded events that span a range of wind and ice conditions.

1. Introduction

In winter, the Arctic Ocean is covered by a consolidated ice pack that moves in response to winds and ocean currents, the response regulated by stress transmission within the ice due to ice-coast and ice-ice interactions. Breakout events occur when the ice pack tears away from its coastal boundaries, experiencing sustained drift and lead opening. Predicting breakouts is of importance to those navigating or working on the consolidated ice pack.

In 2013, an exceptional sea ice breakout in the Beaufort Sea (BS) attracted public attention (The cracks of dawn, 2013). This event has been simulated with the neXtSIM model by Rheinlænder et al. (2022). They find the location and timing of lead opening during the breakout is sensitive to choice of atmospheric model used to force the ice. To our knowledge, this is the first time lead opening and subsequent breakout has been simulated with an accuracy that may allow synoptic forecasts suitable for predicting risk of fracturing during BS ice navigation. Based on their simulations, Rheinlænder et al. (2022) highlighted strong winds and thin ice as key factors for breakout and postulated increases in future breakout frequency as sea ice thins.

In this commentary of Rheinlænder et al. (2022), we highlight the atmospheric synoptic conditions that drove the 2013 breakout and explain the relationship between anticyclone track and the formation of wide leads visible in satellite imagery. We put the 2013 breakout into the context of similar events observed over the satellite record, including years with thicker ice packs. We demonstrate how observations highlight the role of wind direction in determining patterns of lead opening and timing of transition to breakout. Furthermore, we discuss case studies that could be used to test the performance of models such as neXtSIM across a range of conditions.

Writing – review & editing: MacKenzie E. Jewell, Jennifer K. Hutchings

2. Typical Beaufort Breakout Sequence

During winter and spring, anticyclones produce meridional pressure gradients and easterly winds over the BS, opening leads along the Alaskan coast. The leads typically extend offshore toward the center of the passing anticyclone, bounding regions of enhanced fracturing (breakup) and ice drift where the ice pack loses contact with the coast.

In a typical breakout sequence, an eastward-traveling anticyclone strengthens easterly winds over the BS, driving a west-to-east progression of lead opening along the coast. Leads are usually contained on the western side of the wind streamline intersecting Point Barrow, Alaska (Figure 1), where ice moves away from the Alaskan coast, while ice motion to the east remains coastally constrained.

In Text S1 and Figure S1 in Supporting Information S1, we relate the zonal position of previously categorized Beaufort coastal lead patterns (Eicken et al., 2005; Lewis & Hutchings, 2019) to ERA5 winds along the 150°W meridian between 70–75°N (Hersbach et al., 2018). This shows the eastward progression of leads preceding breakout (and breakout timing) relates to the direction of wind forcing relative to the Alaskan coastline. Northeasterly winds form the westernmost patterns: wide arched leads termed Wide Beaufort Arches that extend northward from Point Barrow (Figure 1l). Sustained increases in zonal wind forcing shift winds counterclockwise, driving an eastward progression across patterns. Tangent (TA) leads extend offshore parallel to the Chukchi Coast (Figure 1r), Wide Angle (Figure 1n) then High Angle leads extend from the central and eastern coast of Alaska, respectively. Once easterly winds extend over the BS, an East Coastal (EC) flaw lead (Figure 1t) opens parallel to Banks Island at the eastern boundary of the BS. These leads mark the transition to breakout in which the entire ice pack detaches from the coasts and accelerates. Breakout duration, ranging from a day to weeks, can be measured by EC lead persistence.

When EC leads open, the median easterly wind component and meridional pressure gradient are nearly three times their median winter values (Text S1 in Supporting Information S1). These synoptic conditions can therefore signal the forcing required to initiate most breakouts. Wind speed also increases with eastward lead propagation, and winds are typically 30% faster than usual when EC leads open. However, it may be that winds tend to strengthen as they shift easterly during breakout, but strong winds are not necessarily required for breakout. Easterly winds are on average 40% faster than northerly, southerly, and westerly winds in this region regardless of lead activity. Wind speed does influence subsequent breakout magnitude, which can be characterized by BS ice volume export, drift speeds, and breakup.

3. The 2013 Breakout and Context From Historical Events

From late February through early March of 2013, high sea level pressure and strong anticyclonic winds persisted over the Pacific Arctic. Under this continuous forcing, a series of leads propagated eastward along the Alaskan coast, resulting in breakout (Figures 1q–1t and 2, Movie S1). Progression from western lead activity to breakout began 24 February, coinciding with reductions in against-coast forcing and persistent zonal forcing as winds shifted easterly and weakened (Figures 2a and 2b). The breakout sequence is described in detail in Text S2 in Supporting Information S1.

Breakouts are common in winter (January–April), and the lead opening sequence and rate of ice flux during the 2013 breakout were comparable to events from other years (e.g., 1998 and 2008 in Figure 12 of Babb et al., 2019). However, the record persistence of synoptic forcing in 2013 resulted in exceptional ice dynamics, contributing to the largest March ice flux out of the BS from 1979 to 2016 (Babb et al., 2019).

Beginning 20 February, the meridional sea level pressure difference (ΔP) between 70–75°N along 150°W exceeded 11.5 hPa (a standard deviation above the mean) for 18 consecutive days (Figure 2c). Wind speeds exceeded a standard deviation above the mean (8 m s^{-1}) for 17 days (Figure 2b). For context, Figure 2f shows the distribution of $\Delta P > 11.5$ hPa durations during winters 1993–2013, demonstrating that the 2013 synoptic event lasted nine times longer than the median. It was the longest event of winters 1979–2021 (Table S1 in Supporting Information S1).

TA and EC leads were the most common lead patterns during the transition to breakout in 2013, remaining open for 5 and 14 consecutive days, respectively (Figure 2a). The EC lead persisted longer than the 95th percentile

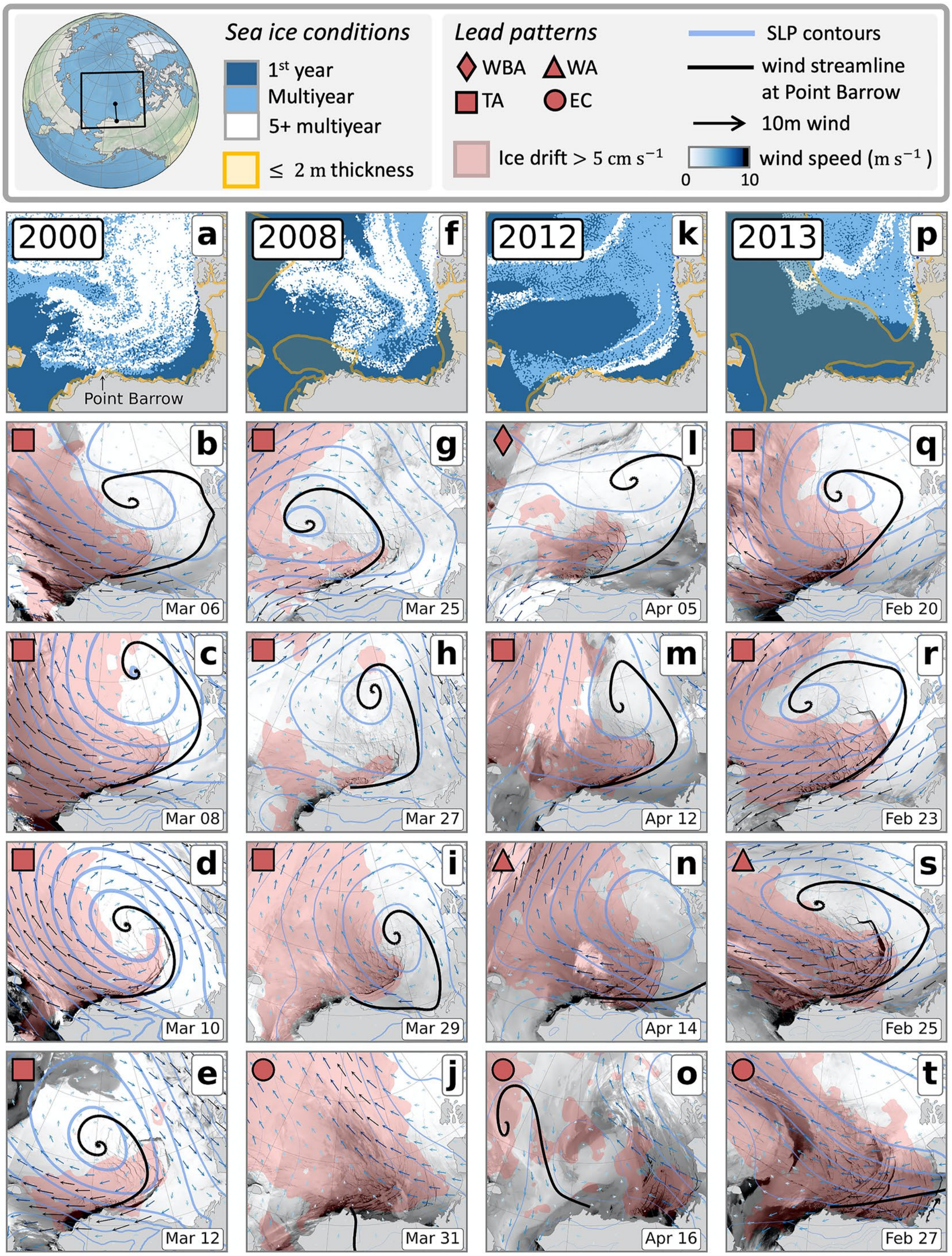

Figure 1. Composite of imagery and observational/reanalysis products during coastal lead opening events. Thermal infrared MODIS imagery of the Beaufort Sea during the 2013 breakout (q–t) and similar events in 2000 (b–e), 2008 (g–j), and 2012 (l–o). Daily average ERA5 sea level pressure (Hersbach et al., 2018) contours overlain every 4 hPa, increasing thickness with magnitude. Ten-meter wind vectors have speed indicated by colorscale. Black line shows the wind streamline intersecting Point Barrow. Daily NSIDC ice drift speeds exceeding 5 cm s^{-1} shaded in pink (Tschudi et al., 2019b). Lead patterns labeled with red symbols. NSIDC ice age maps (Tschudi et al., 2019a) shown for each event (a, f, k, and p), with regions of PIOMAS sea ice thickness ≤2 m shaded yellow (Zhang & Rothrock, 2003). Black box on inset map shows region of interest and black line shows meridian 150°W.

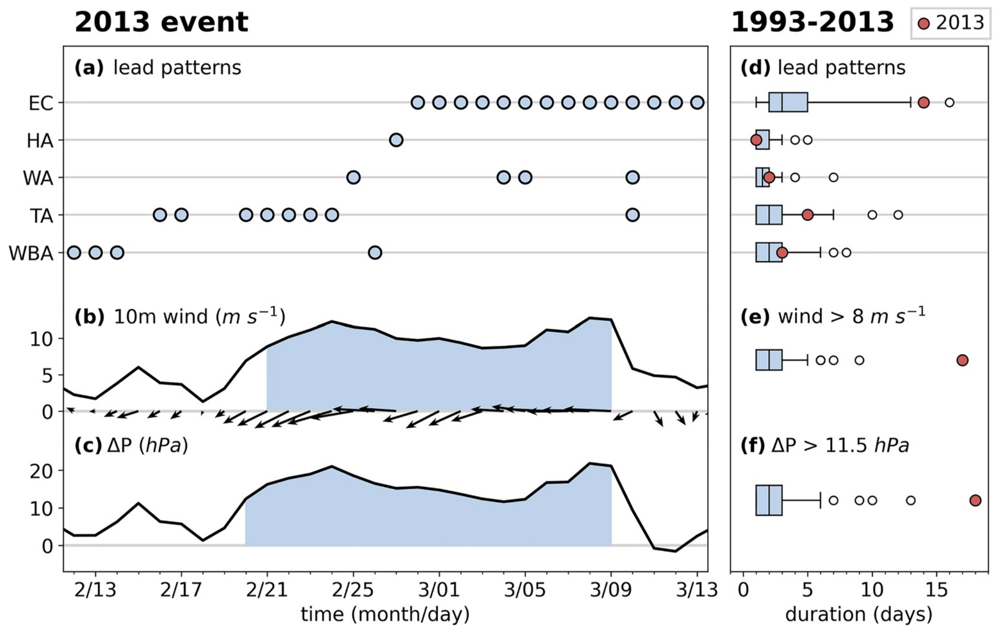

Figure 2. *Left*: 2013 breakout. (a) Lead patterns (Lewis & Hutchings, 2019), from westernmost (Wide Beaufort Arches) to easternmost (East Coastal). Daily average ERA5 10-m wind speed and vectors (b) and pressure difference (c) along meridian 150°W between 70–75°N. Wind speed >8 m s^{-1} and ΔP > 11.5 hPa highlighted in blue. *Right*: Box plots showing January–April 1993–2013 durations of (d) specified lead patterns, (e) wind speed >8 m s^{-1}, and (f) ΔP > 11.5 hPa. Boxes show 25th, 50th, and 75th percentiles. Whiskers show 5th and 95th percentiles. White dots exceed the 95th percentile. Red dots show 2013 breakout maximums.

of 1993–2013 winter durations (Figure 2d). Many similar lead progressions and breakout events have occurred throughout the satellite record, including during years with thicker ice packs than in 2013. Table S2 in Supporting Information S1 lists comparable lead sequences from 1993 to 2013.

Figure 1 shows similar events from 2000, 2008, and 2012 that occurred in thicker ice than in 2013 and under a range of wind speeds. These cases and analyses detailed in Text S1 in Supporting Information S1 demonstrate a consistent connection between wind direction and lead opening across events, with eastward lead progression bound by the wind streamline meeting Point Barrow. In 2008, 2012, and 2013, breakout ensued after the streamline flattened zonally, indicating extension of easterly winds across the BS. During the 2000 event, despite winds of comparable strength to 2013, breakout did not follow western lead opening as winds did not shift sufficiently westward.

4. Summary and Recommendations

Rheinlænder et al. (2022) made an important step in investigating the drivers of breakout by simulating the record-setting 2013 event. The neXtSIM model demonstrated remarkable qualitative correspondence with observed patterns of lead progression and associated ice acceleration during the 2013 breakout (detailed in Text S3 and Figures S2–S5 in Supporting Information S1). Rheinlænder et al. (2022) also simulated alternative breakout progressions with varying ice thicknesses and synoptic forcing products (Figures S2–S5 in Supporting Information S1). Based on the simulations, they indicated that wind speed may control the timing of breakout progression and hypothesized future increases in breakout frequency as sea ice thins.

Observations of previous breakouts over the two decades preceding and including 2013 offer additional insight. We show breakouts have occurred under weaker winds and in thicker ice than in 2013. There are also cases of breakout not occurring under winds of similar strength to 2013 when they were unfavorably oriented toward the coast. These observations demonstrate the challenges in evaluating breakout sensitivity to wind and ice conditions in a model.

Composites of satellite imagery, reanalysis, and observational products presented here offer visualizations of additional cases of breakout, highlighting how changes in wind direction with anticyclone position influence lead progression during breakout. Lead progression during the 2013 Beaufort breakout event followed the typical breakout sequence. However, owing to record persistence of strong easterly wind forcing, the subsequent ice export during this event was exceptional.

Spatiotemporal discontinuities in sea ice drift associated with lead opening are a defining characteristic of winter ice motion in the BS. While the 2013 breakout was associated with thin ice and strong persistent winds, breakouts occur under a range of conditions. Skillful predictions of breakout and its impacts on winter sea ice transport require model validation across a range of conditions. Records of similar sequences of lead opening from 1993 to 2013 (Table S2 in Supporting Information S1) and synoptic events from 1979 to 2021 (Table S1 in Supporting Information S1) span a range of ice thickness distributions and wind forcing patterns.

Simulation of these additional events would test performance of sea ice dynamic models across a range of conditions. Quantitative metrics are needed to assess skill in simulating the location and timing of lead opening, and associated patterns of sea ice drift in response to wind forcing patterns. neXtSIM simulations and observations suggest that for accurate simulation of Beaufort breakouts the atmospheric forcing must capture the location, track, and extent of anticyclones well. Small offsets in anticyclonic forcing can result in large errors in the location of lead formation and hence ice drift. While this is challenging for models, the neXtSIM team demonstrate it is possible.

Data Availability Statement

The neXtSIM model output (Rheinlænder, 2022) is available at https://doi.org/10.5281/zenodo.5639492. NSIDC Polar Pathfinder sea ice drift (Tschudi et al., 2019b) is available at https://doi.org/10.5067/INAWUWO7QH7B and sea ice age (Tschudi et al., 2019a) is available at https://doi.org/10.5067/UTAV7490FEPB. PIOMAS reanalysis sea ice thickness data (Zhang & Rothrock, 2003) is available at http://psc.apl.washington.edu/zhang/IDAO/data_piomas.html. Leads identified by Lewis and Hutchings (2019) are provided at https://doi.org/10.1029/2018JC014898. Leads derived from MODIS imagery (Willmes & Heinemann, 2015b, 2015c) are available at https://doi.org/10.1594/PANGAEA.854411 (Willmes & Heinemann, 2015a). MODIS imagery (MODIS Characterization Support Team (MCST), 2017) is available at http://doi.org/10.5067/MODIS/MOD021KM.061. ERA5 atmospheric reanalysis (Hersbach et al., 2018) is available at https://doi.org/10.24381/cds.adbb2d47.

Acknowledgments

The authors were supported by NASA (80NSSC18K1026 and 80NSSC21K1601) and ONR (N000141912604) Grants. Conversations with Lew Shapiro and Ben Lewis introduced the correspondence between Beaufort lead patterns and the progression of anticyclones. Thanks to Jonathan Rheinlænder and Einar Ólason for sharing model output and information that furthered discussion started in Rheinlænder et al. (2022).

References

Babb, D. G., Landy, J. C., Barber, D. G., & Galley, R. J. (2019). Winter sea ice export from the Beaufort Sea as a preconditioning mechanism for enhanced summer melt: A case study of 2016. *Journal of Geophysical Research: Oceans*, *124*(9), 6575–6600. https://doi.org/10.1029/2019JC015053

Eicken, H., Shapiro, L., Gaylord, A., Mahoney, A., & Cotter, P. (2005). *Mapping and characterization of recurring spring leads and landfast ice in the Beaufort and Chukchi Seas, final report; OCD study BOEM 2005-068* [Technical Report]. US Department of Interior, Minerals Management Service (MMS), Alaska Outer Continental Shelf Region. Retrieved from https://espis.boem.gov/final/ reports/3482.pdf

Hersbach, H., Bell, B., Berrisford, P., Biavati, G., Horányi, A., Muñoz Sabater, J., et al. (2018). ERA5 hourly data on single levels from 1959 to present [Dataset]. Copernicus Climate Change Service (C3S) Climate Data Store (CDS). https://doi.org/10.24381/cds.adbb2d47

Lewis, B. J., & Hutchings, J. K. (2019). Leads and associated sea ice drift in the Beaufort Sea in winter. *Journal of Geophysical Research: Oceans*, *124*(5), 3411–3427. https://doi.org/10.1029/2018JC014898

MODIS Characterization Support Team (MCST). (2017). Modis 1km calibrated radiances product [Dataset]. NASA MODIS Adaptive Processing System, Goddard Space Flight Center. https://doi.org/10.5067/MODIS/MOD021KM.061

Rheinlænder, J. W. (2022). nextsim-data-breakup2013-beaufortsea [Dataset]. Zenodo. https://doi.org/10.5281/zenodo.5639492

Rheinlænder, J. W., Davy, R., Ólason, E., Rampal, P., Spensberger, C., Williams, T. D., et al. (2022). Driving mechanisms of an extreme winter sea ice breakup event in the Beaufort Sea. *Geophysical Research Letters*, *49*(12), e2022GL099024. https://doi.org/10.1029/2022GL099024

The cracks of dawn. (2013). Retrieved from https://neven1.typepad.com/blog/2013/03/the-cracks-of-dawn.html#more

Tschudi, M., Meier, W. N., Stewart, J. S., Fowler, C., & Maslanik, J. (2019a). Ease-grid sea ice age, version 4 [Dataset]. NASA National Snow and Ice Data Center Distributed Active Archive Center. https://doi.org/10.5067/UTAV7490FEPB

Tschudi, M., Meier, W. N., Stewart, J. S., Fowler, C., & Maslanik, J. (2019b). Polar pathfinder daily 25 km ease-grid sea ice motion vectors, version 4 [Dataset]. NASA National Snow and Ice Data Center Distributed Active Archive Center. https://doi.org/10.5067/INAWUWO7QH7B

Willmes, S., & Heinemann, G. (2015a). Daily pan-Arctic sea-ice lead maps for 2003-2015, with links to maps in NetCDF format [Dataset]. Pangaea. https://doi.org/10.1594/PANGAEA.854411

Willmes, S., & Heinemann, G. (2015b). Pan-Arctic lead detection from MODIS thermal infrared imagery. *Annals of Glaciology*, *56*(69), 29–37. https://doi.org/10.3189/2015AoG69A615

Willmes, S., & Heinemann, G. (2015c). Sea-ice wintertime lead frequencies and regional characteristics in the Arctic, 2003–2015. *Remote Sensing*, *8*(1), 4. https://doi.org/10.3390/rs8010004

Zhang, J., & Rothrock, D. (2003). Modeling global sea ice with a thickness and enthalpy distribution model in generalized curvilinear coordinates. *Monthly Weather Review*, *131*(5), 845–861. https://doi.org/10.1175/1520-0493(2003)131<0845:MGSIWA>2.0.CO;2